2024 IEEE/RSJ International Conference on Intelligent Robots and Systems (IROS)
October 14-18, 2024. Abu Dhabi, UAE

Task-Oriented Design Method for Monolithic Flexible Hands with Wire Drive Systems

Rina Kusuhara and Mitsuru Higashimori

***Abstract*— This paper discusses a novel task-oriented design method for wire-driven flexible hands. For a monolithic hand fabricated using 3D printing, an analytical design method is proposed to enable it to perform the given tasks. First, the wiring-synergy equation, which relates the parameters of the hand mechanism, the wire tension, and the generated posture is derived based on an analytical model of a hand with wire drive systems. Next, the posture-synergy equation is derived, using principal component analysis for multiple desired postures given to perform a task. Based on the isomorphism of the mathematical structure in the two synergy equations, a method for designing a hand is developed. By quantitatively evaluating the posture reproducibility with respect to the number of wire drive systems, this method can analytically determine the mechanism parameters and wire tension for the desired postures. Subsequently, the proposed method is validated through case studies. Finally, a hand for an in-hand manipulation task is developed, and the feasibility of the proposed method is validated experimentally. The method potentially contributes to expediting the design procedure, increasing the accuracy of the posture reproduction, and reducing the number of actuators.**

I. Introduction

Hands and grippers are necessary end-effectors for robots to perform task on behalf of or in cooperation with humans. Conventionally, rigid hands fabricated from metal parts have been mainly discussed [1][2]. Recently, soft or flexible robotic hands, utilizing the mechanical characteristics of flexible materials, have been being studied extensively [3][4]. Flexible fingers deform passively and adaptively to the shape and size of an object, which compensates for the shape recognition and locational errors. The posture of such flexible hands is often controlled using pneumatic [5]–[7] and wire drive systems [8]–[13]. In the wire drive system, by applying external tension to the wires passing through the flexible fingers, the driving force is transmitted to the fingers through the passage points of the wire and the posture changes accordingly. Multiple systems can be easily implemented, by which the fingers are expected to generate various postures [10][11]. In addition, 3D printing is increasingly being used to print flexible finger links and joints directly and fabricate hands rapidly [12][13]. This study focuses on the wire drive system, which has the above-mentioned characteristics.

Think about grasping an object with a wire-driven flexible hand. As mentioned earlier, a flexible hand can adaptively deform for various objects and grasp them with a simple mechanism and control. Now, we consider performing tasks such as in-hand manipulation to make the hand more dexterous. In this case, the postures and movements required of the hands become more complex and diverse. Fig. 1(a) shows the general design approach for flexible hands. The design parameters of the hands, i.e., the finger structure, elasticity, wire passages, etc., are determined empirically or experimentally, with emphasis on versatility. Generally, a simple straight finger structure and regular straight wire passages are employed, and wire drive actuators are deployed in sufficient numbers per finger. After the hand is designed, the generated postures and performing tasks are investigated by changing the wire tension as a control input. This approach solves a direct problem, where the task is determined from the predesigned hand parameters. In contrast, recently, novel task-oriented design and fabrication methods have been developed, which utilize 3D printing to fabricate complex monolithic finger structures. Methods for designing finger link structures or wire passages, which aim to reproduce desired postures given to perform tasks, were developed [14][15]. Considering the finger joint elasticity that would be suitable for a given task, a method for designing wave-like joint structures was developed [16]. These methods can be regarded as an approach that solve an inverse problem, where the hand parameters are designed from the target task, as shown in Fig. 1(b). By focusing on a specific task, this approach is expected to have the advantages of reproducing the desired postures with high accuracy and reducing the number of actuators. This study adopts such a task-oriented design approach. In our previous work [17], the analytical design method for a single finger with wire drive systems

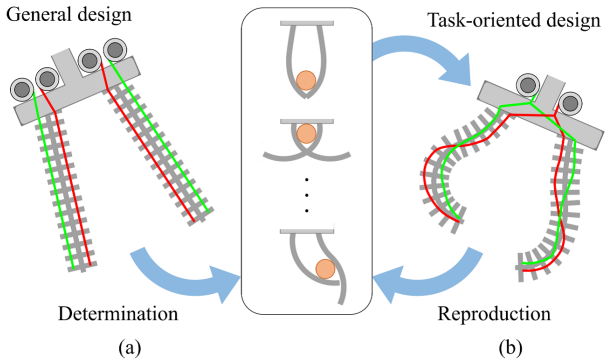

Fig. 1. Toward performing a task. (a) General approach. The direct problem, in which the hand postures for a given task are determined under a predesigned general hand, is solved. (b) Task-oriented approach. The inverse problem, in which a hand is designed to reproduce the hand postures for a given task, is solved. By focusing on a specific task, a high accuracy with fewer actuators can be expected.

*This work was supported in part by JSPS KAKENHI Grant Number JP24K00850.

R. Kusuhara and M. Higashimori are with the Department of Mechanical Engineering, Graduate School of Engineering, Osaka University, Suita 565-0871, Japan. kusuhara@ims.mech.eng.osaka-u.ac.jp, higashi@mech.eng.osaka-u.ac.jp

was explored based on the concept of hardware synergy [18]. Extending that work, this study presents a design problem for a whole hand with multiple fingers as shown in Fig. 1(b).

Based on the abovementioned background, this paper presents a novel task-oriented design for wire-driven flexible hands. For a monolithic hand fabricated using 3D printing, an analytical design method is proposed, which is intended for reproducing the desired postures given to perform specific tasks. First, an analytical model of the hand is introduced, based on which the wiring-synergy equation, which relates the mechanism parameters, wire tension, and generated posture, is derived. Next, the task-oriented design method is explained. For multiple desired postures required for a task, the posture-synergy equation is derived using principal component analysis (PCA). Based on the isomorphism of the mathematical structure in the two synergy equations, a method for designing the hand is developed. By quantitatively evaluating the reproducibility of the desired postures with respect to the number of wire drive systems, this method can analytically determine the mechanism parameters and wire tension for the desired postures. Subsequently, the proposed method is validated through case studies in which hands for multi-mode grasping, in-hand manipulation, and both of these tasks are respectively designed. Finally, a hand for the in-hand manipulation task is developed. The feasibility of the proposed method is validated experimentally via reproducing the postures and performing the task. The proposed method potentially contributes to expediting the design procedure, increasing the accuracy of the posture reproduction, and reducing the number of actuators.

II. Analytical Hand Model

This section defines an analytical model for hand with wire drive systems. The wiring-synergy equation, which relates the mechanism parameters, wire tension, and generated posture, is derived.

A. Monolithic Hand with Wire Drive Systems

Fig. 2(a) shows an outline of hand dealt in this paper, where the hand is monolithically fabricated by 3D printing. The hand comprises fingers, palm, wires, and actuators that generate tension. Each finger is elastic, and it has a trunk and branches. The root of each finger's trunk is connected to the palm, and the trunk undergoes only bending deformation. Each branch has a passage for a wire. The wire passes through all the passages, one end of which is fixed at the tip branch. The other end is combined to those for the other fingers at the palm. Furthermore, by connecting the combined part and the wire pulled by an actuator, a wire drive system (WDS) is formed. When tension is given by the actuator, each trunk undergoes a bending moment via the passages for the wire. Thus, whole hand posture changes. It returns to the natural posture owing to the elasticity when the tension is removed. Multiple WDSs can be implemented on the hand, and various hand postures are generated by the synergy of WDSs.

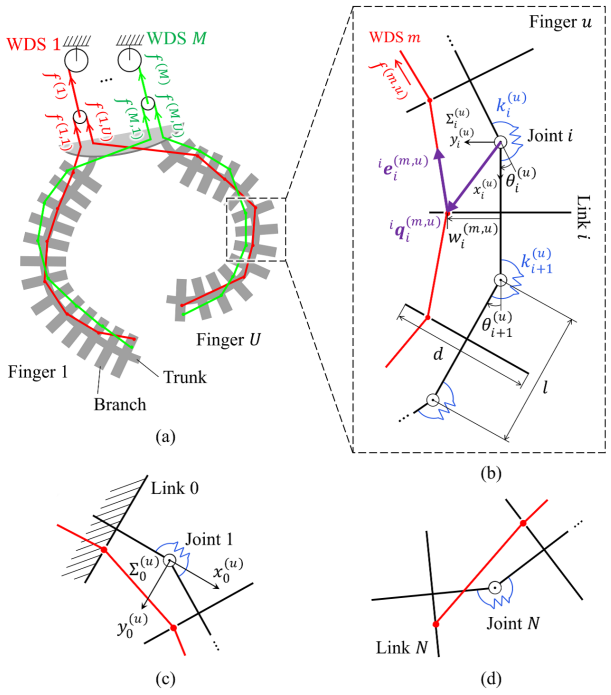

Fig. 2. Monolithic hand with wire drive systems. (a) Outline. (b) Analytical model of a finger. (c) Root of the finger. (d) Tip of the finger.

B. Analytical Model

For the hand shown in Fig. 2(a), we introduce a two-dimensional analytical model. The number of fingers is U and each finger is denoted as finger u ($u = 1, \cdots, U$). Suppose that the fingers do not interfere each other and the mass of the finger is sufficiently small so that deformation due to its self-weight does not occur. The palm is fixed to the absolute coordinate system. The number of WDSs is M and each WDS is denoted as WDS m ($m = 1, \cdots, M$). Figs. 2(b)–(d) show a discretized analytical model for the hand. The center point on the trunk between two branches is considered a virtual rotational joint. The branch and trunk between two joints are considered a virtual cross-shaped rigid link. The bending elasticity of the trunk is replaced by a torsion spring at a virtual joint. Hereinafter, the virtual link and joint are simply called link and joint. Each finger has $N+1$ links. As shown in Fig. 2(c), link 0 is the root link fixed at the palm, i.e., base. As shown in Fig. 2(d), Link N is the tip link. In each link, the branch is located at the center of the trunk, and the branch and trunk are perpendicular to each other. The link width is negligibly small. As shown in Fig. 2(b), joint i ($i = 1, \cdots, N$) connects link $i-1$ and link i. The passage for the wire is sufficiently small to be considered a point. The friction between the wire and passage is negligible. This means that the wire tension on finger is uniform in WDS m. The symbols in Fig. 2 are defined as follows:

- $\Sigma_0^{(u)}$ Base coordinate system in which the origin is located at the rotational axis of joint 1 on finger u. The $x_0^{(u)}$- and $y_0^{(u)}$-axes are the trunk and branch directions of link 0, respectively.
- $\Sigma_i^{(u)}$ Coordinate system in which the origin is located at

the rotational axis of joint i on finger u. The $x_i^{(u)}$- and $y_i^{(u)}$-axes are the trunk and branch directions of link i, respectively.

d Branch length of a link.

l Trunk length of a link.

$w_i^{(m,u)}$ Passage point for WDS m from the trunk of link i on finger u. $-d/2 < w_i^{(m,u)} < d/2$.

${}^i\boldsymbol{q}_j^{(m,u)}$ Position vector expressing the passage point for WDS m of link j on finger u with respect to $\Sigma_i^{(u)}$.

$k_i^{(u)}$ Torsion spring constant at joint i on finger u.

$\theta_i^{(u)}$ Angular displacement of joint i on finger u, i.e., the angle between the $x_{i-1}^{(u)}$- and $x_i^{(u)}$-axes.

$\theta_{\mathrm{n},i}^{(u)}$ Angular displacement of joint i on finger u with respect to the natural state of the spring at joint i.

$f^{(m)}$ Tension generated by the actuator for WDS m.

$f^{(m,u)}$ Tension given to the wire passing through finger u for WDS m.

${}^i\boldsymbol{e}_i^{(m,u)}$ Direction vector of tension $f^{(m,u)}$ at ${}^i\boldsymbol{q}_i^{(m,u)}$. ${}^i\boldsymbol{e}_i^{(m,u)} = \frac{{}^i\boldsymbol{q}_{i-1}^{(m,u)} - {}^i\boldsymbol{q}_i^{(m,u)}}{\|{}^i\boldsymbol{q}_{i-1}^{(m,u)} - {}^i\boldsymbol{q}_i^{(m,u)}\|}$.

Assume that $f^{(m)}$ generated by the actuator is equally distributed to all finger, namely $f^{(m,u)} = \frac{1}{U} f^{(m)}$. A mechanism to realize this assumption is introduced in Section V.

C. Wiring-Synergy Equation

For finger u, the torque generated at each joint by M WDSs is expressed as follows:

$$\boldsymbol{\tau}_{\mathrm{f}}^{(u)} = \boldsymbol{W}^{(u)} \boldsymbol{f}^{(u)}, \tag{1}$$

$$\boldsymbol{W}^{(u)} = \begin{bmatrix} {}^1\boldsymbol{q}_1^{(1,u)} \otimes {}^1\boldsymbol{e}_1^{(1,u)} & \cdots & {}^1\boldsymbol{q}_1^{(M,u)} \otimes {}^1\boldsymbol{e}_1^{(M,u)} \\ \vdots & \ddots & \vdots \\ {}^N\boldsymbol{q}_N^{(1,u)} \otimes {}^N\boldsymbol{e}_N^{(1,u)} & \cdots & {}^N\boldsymbol{q}_N^{(M,u)} \otimes {}^N\boldsymbol{e}_N^{(M,u)} \end{bmatrix},$$

$$\boldsymbol{f}^{(u)} = \left[f^{(1,u)}, \cdots, f^{(M,u)} \right]^{\mathrm{T}},$$

where $\otimes$ denotes the operator providing $\boldsymbol{x} \otimes \boldsymbol{y} = x_1 y_2 - x_2 y_1$ for $\boldsymbol{x} = [x_1, x_2]^{\mathrm{T}}$ and $\boldsymbol{y} = [y_1, y_2]^{\mathrm{T}}$. Meanwhile, the restoring torque generated by the elasticity according to angular displacement $\theta_i^{(u)}$ is expressed as follows:

$$\boldsymbol{\tau}_{\mathrm{k}}^{(u)} = -\boldsymbol{E}^{(u)} \left(\boldsymbol{\theta}^{(u)} - \boldsymbol{\theta}_{\mathrm{n}}^{(u)} \right), \tag{2}$$

$$\boldsymbol{E}^{(u)} = \mathrm{diag} \left[k_1^{(u)}, \cdots, k_N^{(u)} \right],$$

$$\boldsymbol{\theta}^{(u)} = \left[\theta_1^{(u)}, \cdots, \theta_N^{(u)} \right]^{\mathrm{T}}, \quad \boldsymbol{\theta}_{\mathrm{n}}^{(u)} = \left[\theta_{\mathrm{n},1}^{(u)}, \cdots, \theta_{\mathrm{n},N}^{(u)} \right]^{\mathrm{T}}.$$

Considering a quasi-static condition in which the torque given by (1) and (2) are equilibrate constantly, the following equation is obtained:

$$\boldsymbol{\tau}_{\mathrm{f}}^{(u)} + \boldsymbol{\tau}_{\mathrm{k}}^{(u)} = \boldsymbol{W}^{(u)} \boldsymbol{f}^{(u)} - \boldsymbol{E}^{(u)} \left(\boldsymbol{\theta}^{(u)} - \boldsymbol{\theta}_{\mathrm{n}}^{(u)} \right) = \boldsymbol{0}. \tag{3}$$

For the detailed derivation process of (1)–(3), see [17] that analyzed a single finger. In this paper, (3) is expanded for multi-fingered hands. The hand posture is expressed by

$$\boldsymbol{\theta} = \begin{bmatrix} \boldsymbol{\theta}^{(1)} \\ \vdots \\ \boldsymbol{\theta}^{(U)} \end{bmatrix} = \begin{bmatrix} \theta_1 \\ \vdots \\ \theta_{UN} \end{bmatrix}. \tag{4}$$

Generalizing (3) for U fingers based on the assumption of $f^{(m,u)} = \frac{1}{U} f^{(m)}$, the following relation is obtained:

$$\frac{1}{U} \boldsymbol{W} \boldsymbol{f} - \boldsymbol{E} \left(\boldsymbol{\theta} - \boldsymbol{\theta}_{\mathrm{n}} \right) = \boldsymbol{0}, \tag{5}$$

$$\boldsymbol{W} = \begin{bmatrix} \boldsymbol{W}^{(1)} \\ \vdots \\ \boldsymbol{W}^{(U)} \end{bmatrix}, \ \boldsymbol{E} = \begin{bmatrix} \boldsymbol{E}^{(1)} & & \boldsymbol{0} \\ & \ddots & \\ \boldsymbol{0} & & \boldsymbol{E}^{(U)} \end{bmatrix}, \ \boldsymbol{\theta}_{\mathrm{n}} = \begin{bmatrix} \boldsymbol{\theta}_{\mathrm{n}}^{(1)} \\ \vdots \\ \boldsymbol{\theta}_{\mathrm{n}}^{(U)} \end{bmatrix},$$

$$\boldsymbol{f} = \left[f^{(1)}, \cdots, f^{(M)} \right]^{\mathrm{T}},$$

where the wiring matrix $\boldsymbol{W} \in \mathbb{R}^{UN \times M}$, the elasticity matrix $\boldsymbol{E} \in \mathbb{R}^{UN \times UN}$. Based on the definition of ${}^i\boldsymbol{e}_i^{(m,u)}$ and (1), each component of the wiring matrix $\boldsymbol{W}$ is given by

$$W_{i,m}^{(u)} = \frac{{}^i\boldsymbol{q}_i^{(m,u)} \otimes ({}^i\boldsymbol{q}_{i-1}^{(m,u)} - {}^i\boldsymbol{q}_i^{(m,u)})}{\|{}^i\boldsymbol{q}_{i-1}^{(m,u)} - {}^i\boldsymbol{q}_i^{(m,u)}\|}, \tag{6}$$

where the following is constantly given:

$${}^i\boldsymbol{q}_i^{(m,u)} = \begin{bmatrix} \frac{l}{2} \\ w_i^{(m,u)} \end{bmatrix}. \tag{7}$$

If the links are sufficiently numerous, each angular displacement $\theta_i^{(u)}$ can be considered minute although the entire finger bends. Based on this assumption, the position vector included in (6), which is a nonlinear function of $\theta_i^{(u)}$, is replaced as

$${}^i\boldsymbol{q}_{i-1}^{(m,u)} = \begin{bmatrix} \cos\theta_i^{(u)} & \sin\theta_i^{(u)} \\ -\sin\theta_i^{(u)} & \cos\theta_i^{(u)} \end{bmatrix} \begin{bmatrix} -\frac{l}{2} \\ w_{i-1}^{(m,u)} \end{bmatrix} \approx \begin{bmatrix} -\frac{l}{2} \\ w_{i-1}^{(m,u)} \end{bmatrix}. \tag{8}$$

Substituting (7) and (8) into (6), the component of $\boldsymbol{W}$ is expressed as follows:

$$W_{i,m}^{(u)} = \frac{\begin{bmatrix} \frac{l}{2} \\ w_i^{(m,u)} \end{bmatrix} \otimes \begin{bmatrix} -l \\ w_{i-1}^{(m,u)} - w_i^{(m,u)} \end{bmatrix}}{\sqrt{l^2 + \left(w_{i-1}^{(m,u)} - w_i^{(m,u)} \right)^2}}, \tag{9}$$

which is the function of only the passage point $w_i^{(m,u)}$. From (5), the following equation is obtained:

$$\boldsymbol{\theta} = \frac{1}{U} \boldsymbol{E}^{-1} \boldsymbol{W} \boldsymbol{f} + \boldsymbol{\theta}_{\mathrm{n}} \quad (\boldsymbol{f} \geq \boldsymbol{0}). \tag{10}$$

Considering (9), (10) expresses the whole hand posture $\boldsymbol{\theta}$ generated for the tension $\boldsymbol{f}$ given by actuators under the mechanism parameters $\boldsymbol{W}$, $\boldsymbol{\theta}_{\mathrm{n}}$, and $\boldsymbol{E}$. Hereinafter, (10) is referred to as the wiring-synergy equation. Note that each component of the tension $\boldsymbol{f}$ is non-negative.

Equation (10) can be utilized to solve the direct problem, i.e., to determine postures for performing tasks from the design parameters. In this paper, (10) is utilized to solve the inverse problem.

III. Task-Oriented Design Method

After defining the posture-synergy equation for desired postures by using PCA, an analytical design method is constructed based on the two synergy equations[1].

A. Principal Component Analysis for Desired Postures

Suppose H desired postures are given to perform a task, as shown in Fig. 3(a). Desired posture h is represented as $\boldsymbol{\theta}_{\mathrm{r}h} = [\theta_{\mathrm{r}h,1}, \cdots, \theta_{\mathrm{r}h,UN}]^{\mathrm{T}}$ $(h = 1, \cdots, H)$. $\boldsymbol{\theta}_{\mathrm{r}h}$ is centralized as follows:

$$\hat{\boldsymbol{\theta}}_{\mathrm{r}h} = \left[\hat{\theta}_{\mathrm{r}h,1}, \cdots, \hat{\theta}_{\mathrm{r}h,UN}\right]^{\mathrm{T}}, \tag{11}$$

$$\hat{\theta}_{\mathrm{r}h,i} = \theta_{\mathrm{r}h,i} - \bar{\theta}_{\mathrm{r},i}, \quad \bar{\theta}_{\mathrm{r},i} = \frac{1}{H}\sum_{h=1}^{H} \theta_{\mathrm{r}h,i}. \tag{12}$$

Applying PCA to all of $\hat{\boldsymbol{\theta}}_{\mathrm{r}h}$, we obtain the following equation:

$$\hat{\boldsymbol{\theta}} = \boldsymbol{S}\boldsymbol{\sigma}, \tag{13}$$
$$\boldsymbol{S} = [\boldsymbol{s}_1, \cdots, \boldsymbol{s}_{UN}],$$

where $\boldsymbol{s}_i \in \mathbb{R}^{UN}$ is the direction vector of the i-th principal component, $\boldsymbol{\sigma} \in \mathbb{R}^{UN}$ is the principal component vector, and $\hat{\boldsymbol{\theta}}$ is the posture in the centralized space. The relationship between $\hat{\boldsymbol{\theta}}$ and $\boldsymbol{\theta}$ is given as

$$\hat{\boldsymbol{\theta}} = \boldsymbol{\theta} - \bar{\boldsymbol{\theta}}_{\mathrm{r}}, \quad \bar{\boldsymbol{\theta}}_{\mathrm{r}} = \left[\bar{\theta}_{\mathrm{r},1}, \cdots, \bar{\theta}_{\mathrm{r},UN}\right]^{\mathrm{T}}, \tag{14}$$

where $\bar{\boldsymbol{\theta}}_{\mathrm{r}}$ is the average posture derived from all desired postures. Substituting (14) into (13), the following equation is obtained:

$$\boldsymbol{\theta} = \boldsymbol{S}\boldsymbol{\sigma} + \bar{\boldsymbol{\theta}}_{\mathrm{r}}. \tag{15}$$

Equation (15) expresses the coordinate transformation from $\boldsymbol{\sigma}$ to the posture $\boldsymbol{\theta}$. From (15), $\boldsymbol{\sigma}_{\mathrm{r}h}$ for the desired posture $\boldsymbol{\theta}_{\mathrm{r}h}$ is given by $\boldsymbol{\sigma}_{\mathrm{r}h} = \boldsymbol{S}^{-1}(\boldsymbol{\theta}_{\mathrm{r}h} - \bar{\boldsymbol{\theta}}_{\mathrm{r}})$. Fig. 3(b) shows the coordinate transformation using (15) with respect to $\boldsymbol{\theta}_{\mathrm{r}h}$. λ_i is the variance of the desired postures with respect to the i-th principal component axis. The contribution ratio R_i for the i-th principal component axis, i.e., the proportion of the information presented in the i-th principal component axis out of the total information included in the desired postures, is defined as $R_i = \frac{\lambda_i}{\sum_{j=1}^{UN}\lambda_j}$. In addition, the cumulative contribution ratio, i.e., the proportion of the information presented in the 1st–i-th principal component axes, is defined as $R_{\mathrm{cum},i} = \sum_{j=1}^{i} R_j$.

B. Designing of Hand

1) Posture-Synergy Equation: There exists an analogy of mathematical structure between (10) and (15) which output hand posture $\boldsymbol{\theta}$. Based on this, it can be expected to determine the hand parameters included in (10). However, the following customizations are required.

[1]The derivation of postural correlation patterns (synergies) using PCA has been extensively employed. In hardware implementation of the synergies, the proposed method, which includes the transmission mechanism with movable pulleys for actuating the elastic fingers, is categorized as adaptive synergy defined in [18]. However, the adaptive finger motions to an object is out of scope in this paper.

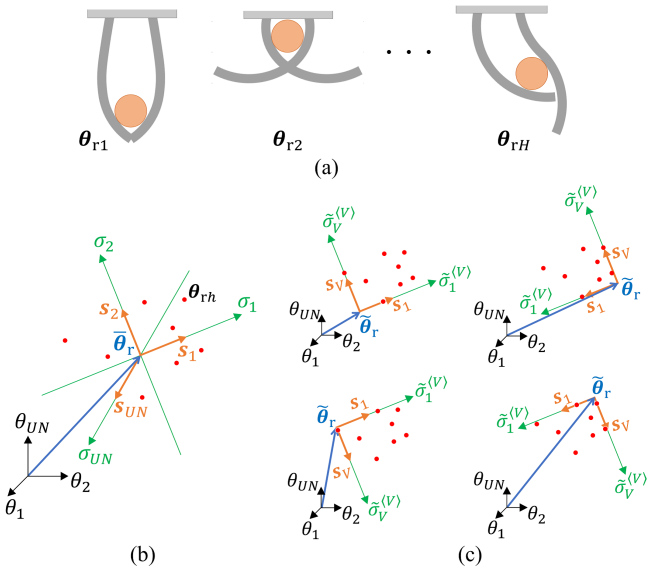

Fig. 3. Mathematical processing of desired postures. (a) Desired postures $\boldsymbol{\theta}_{\mathrm{r}h}$ for a task. (b) $\boldsymbol{\theta}_{\mathrm{r}h}$ in the coordinate system given by (15), which represents the principal component space. (c) $\boldsymbol{\theta}_{\mathrm{r}h}$ in the coordinate system given by (17), which represents the dimension-reduced and non-negative space. There are 2^V systems (the figure shows the case for $V = 2$).

The dimension of tension $\boldsymbol{f}$, which is the input of (10), is the number of WDSs M. Meanwhile, the dimension of the principal component $\boldsymbol{\sigma}$, which is the input of (15), is the total number of links UN, ranging from tens to hundreds. In terms of saving actuators, the number of WDSs M should be as small as possible unless impairing the reproducibility of the desired posture. Therefore, dimensionality reduction based on cumulative contribution ratio is performed for $\boldsymbol{\sigma}$ in (15), which has a correspondence relation with $\boldsymbol{f}$ in (10). The minimum number of inputs by which $R_{\mathrm{cum},i}$ overcomes the threshold R_{th} is expressed as

$$V = \min\{i \mid R_{\mathrm{cum},i} \geq R_{\mathrm{th}}\} \quad (i = 1, \cdots, UN).$$

Using the 1st–V-th columns of $\boldsymbol{S}$ and the 1st–V-th components of $\boldsymbol{\sigma}$ in (15), we obtain the dimension-reduced posture as follows:

$$\boldsymbol{\theta} = \boldsymbol{S}^{\langle V\rangle}\boldsymbol{\sigma}^{\langle V\rangle} + \bar{\boldsymbol{\theta}}_{\mathrm{r}}, \tag{16}$$

where $\boldsymbol{S}^{\langle V\rangle} \in \mathbb{R}^{UN\times V}$ and $\boldsymbol{\sigma}^{\langle V\rangle} \in \mathbb{R}^{V}$. Subsequently, considering that the tension $\boldsymbol{f}$ in (10) has a non-negative range, we transform (16) such that the input $\boldsymbol{\sigma}^{\langle V\rangle}$ in (16) also has a non-negative range. Let $\boldsymbol{\sigma}_{\mathrm{r}h}^{\langle V\rangle} = \left[\sigma_{\mathrm{r}h,1}^{\langle V\rangle}, \cdots, \sigma_{\mathrm{r}h,V}^{\langle V\rangle}\right]^{\mathrm{T}}$ be the 1st–V-th components of $\boldsymbol{\sigma}_{\mathrm{r}h}$. For $\boldsymbol{\sigma}_{\mathrm{r}h}^{\langle V\rangle}$ $(h = 1, \cdots, H)$, consider the minimum value of the v-th components represented as $\sigma_{\mathrm{rmin},v} = \min\{\sigma_{\mathrm{r}1,v}^{\langle V\rangle}, \cdots, \sigma_{\mathrm{r}H,v}^{\langle V\rangle}\}$. Using $\boldsymbol{\sigma}_{\mathrm{rmin}} = [\sigma_{\mathrm{rmin},1}, \cdots, \sigma_{\mathrm{rmin},V}]^{\mathrm{T}}$, (16) is transformed as

$$\boldsymbol{\theta} = \boldsymbol{S}^{\langle V\rangle}\tilde{\boldsymbol{\sigma}}^{\langle V\rangle} + \tilde{\boldsymbol{\theta}}_{\mathrm{r}} \quad (\tilde{\boldsymbol{\sigma}}^{\langle V\rangle} \geq \boldsymbol{0}), \tag{17}$$
$$\tilde{\boldsymbol{\sigma}}^{\langle V\rangle} = \boldsymbol{\sigma}^{\langle V\rangle} - \boldsymbol{\sigma}_{\mathrm{rmin}}, \quad \tilde{\boldsymbol{\theta}}_{\mathrm{r}} = \bar{\boldsymbol{\theta}}_{\mathrm{r}} + \boldsymbol{S}^{\langle V\rangle}\boldsymbol{\sigma}_{\mathrm{rmin}}.$$

The non-negative input $\tilde{\boldsymbol{\sigma}}_{\mathrm{r}h}^{\langle V\rangle}$ for the desired posture $\boldsymbol{\theta}_{\mathrm{r}h}$ is given by $\tilde{\boldsymbol{\sigma}}_{\mathrm{r}h}^{\langle V\rangle} = \boldsymbol{\sigma}_{\mathrm{r}h}^{\langle V\rangle} - \boldsymbol{\sigma}_{\mathrm{rmin}}$. Fig. 3(c) shows the coordinate transformation using (17) with respect to the desired postures. Here, note that owing to the arbitrariness

of positive and negative directions of the principal component axis $\boldsymbol{s}_i$ ($i = 1, \cdots, V$), 2^V different coordinate transformations are obtained. Hereinafter, (17), which has the identical mathematical structure with (10), is referred to as the posture-synergy equation.

2) Determination of Parameters: By referring to (17) for each component, we can analytically determine the parameters of hand mechanism included in (10). First, the number of WDSs is determined using the following equation such that the input $\boldsymbol{f} \in \mathbb{R}^M$ and $\boldsymbol{\sigma}^{\langle V \rangle} \in \mathbb{R}^V$ have the same dimensions:

$$M = V. \tag{18}$$

Next, by comparing the right-hand side of (10) with that of (17), we can obtain the following equations:

$$\boldsymbol{E}^{-1}\boldsymbol{W}\boldsymbol{A} = \boldsymbol{S}^{\langle V \rangle} \quad \rightarrow \quad \boldsymbol{W} = \boldsymbol{E}\boldsymbol{S}^{\langle V \rangle}\boldsymbol{A}^{-1}, \tag{19}$$

$$\frac{1}{U}\boldsymbol{A}^{-1}\boldsymbol{f} = \tilde{\boldsymbol{\sigma}}^{\langle V \rangle} \quad \rightarrow \quad \boldsymbol{f} = U\boldsymbol{A}\tilde{\boldsymbol{\sigma}}^{\langle V \rangle}, \tag{20}$$

$$\boldsymbol{\theta}_{\mathrm{n}} = \tilde{\boldsymbol{\theta}}_{\mathrm{r}}, \tag{21}$$

where $\boldsymbol{A} = \mathrm{diag}[\alpha_1, \cdots, \alpha_M]$ is the coefficient matrix that adjusts the trade-off between the value of the passage point $w_i^{(m,u)}$ in $\boldsymbol{W}$ and the value of the tension $f^{(m)}$ in $\boldsymbol{f}$. Using (19) and (21), the wiring matrix $\boldsymbol{W}$ and natural posture $\boldsymbol{\theta}_{\mathrm{n}}$ are determined, respectively. The passage point $w_i^{(m,u)}$ is given by (9) and (19). Using (20), the tension $\boldsymbol{f}_{\mathrm{r}h}$ to reproduce the desired postures $\boldsymbol{\theta}_{\mathrm{r}h}$ is determined as follows:

$$\boldsymbol{f}_{\mathrm{r}h} = U\boldsymbol{A}\tilde{\boldsymbol{\sigma}}_{\mathrm{r}h}^{\langle V \rangle}. \tag{22}$$

The finger elasticity $\boldsymbol{E}$ is excluded from design. While (19)–(22) are the basic determination rules, the following points should be noted. The coefficient matrix $\boldsymbol{A}$ is required to be determined such that passage point $w_i^{(m,u)}$ in (19) must be on the branch, i.e., $|w_i^{(m,u)}| < d/2$ and tension $\boldsymbol{f}_{\mathrm{r}h}$ in (22) must be less than or equal to the maximum tension $\boldsymbol{f}_{\max}$, i.e., $\boldsymbol{f}_{\mathrm{r}h} \leq \boldsymbol{f}_{\max}$. $\boldsymbol{f}_{\mathrm{r}h}$ should be as small as possible under $\boldsymbol{f}_{\max}$ derived from the actuator specification. As shown in Fig. 3(c), 2^V types of $\tilde{\boldsymbol{\theta}}_{\mathrm{r}}$ are obtained. This means that there exist 2^V candidates for the natural posture $\boldsymbol{\theta}_{\mathrm{n}}$ in (21). One, for which the bend of the finger is as smooth as possible, should be selected as $\boldsymbol{\theta}_{\mathrm{n}}$. As described above, the proposed method determines parameters via mathematical analytical formulae, which may lead to physically inappropriate solutions or even to no solutions. A detailed discussion on the existence and validity of solution is a subject in the future.

IV. Case Studies

In this section, case studies are presented and the validity of the proposed method is verified.

A. Basic Configuration

Fig. 4 shows a basic two-fingered hand model ($U = 2$) used for case studies. Fingers were attached at the palm, and the distance between the fingers was $70\ \mathrm{mm}$. The finger attachment surface of palm sloped symmetrically at $10\ ^\circ$. The length of each finger was $210\ \mathrm{mm}$, and the number of links was $N = 35$. The lengths of the trunk and branch were $l = 6\ \mathrm{mm}$ and $d = 20\ \mathrm{mm}$, respectively. The torsion spring constant was $k_i^{(u)} = 830\ \mathrm{N \cdot mm/rad}$, obtained from the preliminary experiment. While the natural posture of the fingers is depicted as $\boldsymbol{\theta}_{\mathrm{n}} = \boldsymbol{0}$ in Fig. 4, $\boldsymbol{\theta}_{\mathrm{n}}$ for each case study was determined in the design process. The threshold of the cumulative contribution ratio was set as $R_{\mathrm{th}} = 0.95$. The maximum tension was set as $f_{\max} = 52\ \mathrm{N}$.

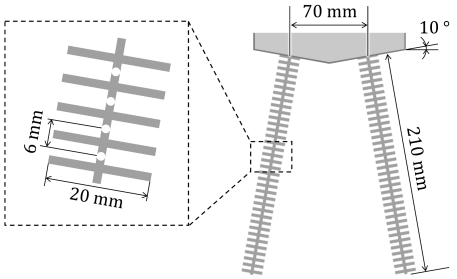

Fig. 4. Basic configuration for designing a hand.

TABLE I
Cumulative contribution ratio in case studies.

	$R_{\mathrm{cum},1}$	$R_{\mathrm{cum},2}$	$R_{\mathrm{cum},3}$	$R_{\mathrm{cum},4}$	$\cdots$	$R_{\mathrm{cum},70}$
Case 1	0.67	<u>0.98</u>	0.99	0.99	$\cdots$	1.0
Case 2	0.61	<u>0.98</u>	0.99	0.99	$\cdots$	1.0
Case 3	0.56	0.86	<u>0.96</u>	0.99	$\cdots$	1.0

B. Case Studies

1) Case 1: Multi-Mode Grasping Task: Assuming a grasping task with multiple modes, we designed a hand for four desired postures $\boldsymbol{\theta}_{\mathrm{r}1}$–$\boldsymbol{\theta}_{\mathrm{r}4}$, as shown in Fig. 5(a). $\boldsymbol{\theta}_{\mathrm{r}1}$–$\boldsymbol{\theta}_{\mathrm{r}3}$ were for three grasping modes and $\boldsymbol{\theta}_{\mathrm{r}4}$ was for releasing. These were all symmetrical hand postures. As shown in TABLE I, in Case 1, the minimum number of inputs overcoming the threshold of cumulative contribution ratio $R_{\mathrm{th}} = 0.95$ was $V = 2$ with $R_{\mathrm{cum},2} = 0.98$; thus, the number of WDSs was determined as $M = 2$. Fig. 5(b) shows the design result. $2^V = 4$ candidates for the natural posture $\boldsymbol{\theta}_{\mathrm{n}}$ were obtained as shown in the top left of Fig. 5(b). TABLE II shows the maximum and average of the absolute angles for all components of $\boldsymbol{\theta}_{\mathrm{n}}$. For the sake of the smooth finger structure, candidate (i), which had the minimum values among all candidates for Case 1 in TABLE II, was selected, as shown in the bottom left of Fig. 5(b). The red and green lines in the bottom left of Fig. 5(b) indicate the passage points for WDS 1 and WDS 2, respectively. The tensions $f^{(1)}$ and $f^{(2)}$ for reproducing the desired postures $\boldsymbol{\theta}_{\mathrm{r}1}$–$\boldsymbol{\theta}_{\mathrm{r}4}$ are shown in the right of Fig. 5(b). The magenta lines show the desired postures, and the blue lines show the reproduced postures obtained by quasi-static simulation using (5). The coefficient matrix was $\boldsymbol{A} = \mathrm{diag}[3.5, 6.3]$.

2) Case 2: In-Hand Manipulation Task: Assuming an in-hand manipulation task, we designed a hand for five desired postures $\boldsymbol{\theta}_{\mathrm{r}4}$–$\boldsymbol{\theta}_{\mathrm{r}8}$, as shown in Fig. 5(a). $\boldsymbol{\theta}_{\mathrm{r}5}$–$\boldsymbol{\theta}_{\mathrm{r}8}$ were for manipulating the object downward, upward, to the left, and to the right, and $\boldsymbol{\theta}_{\mathrm{r}4}$ was for releasing. Asymmetrical hand postures were included, which were not present in Case

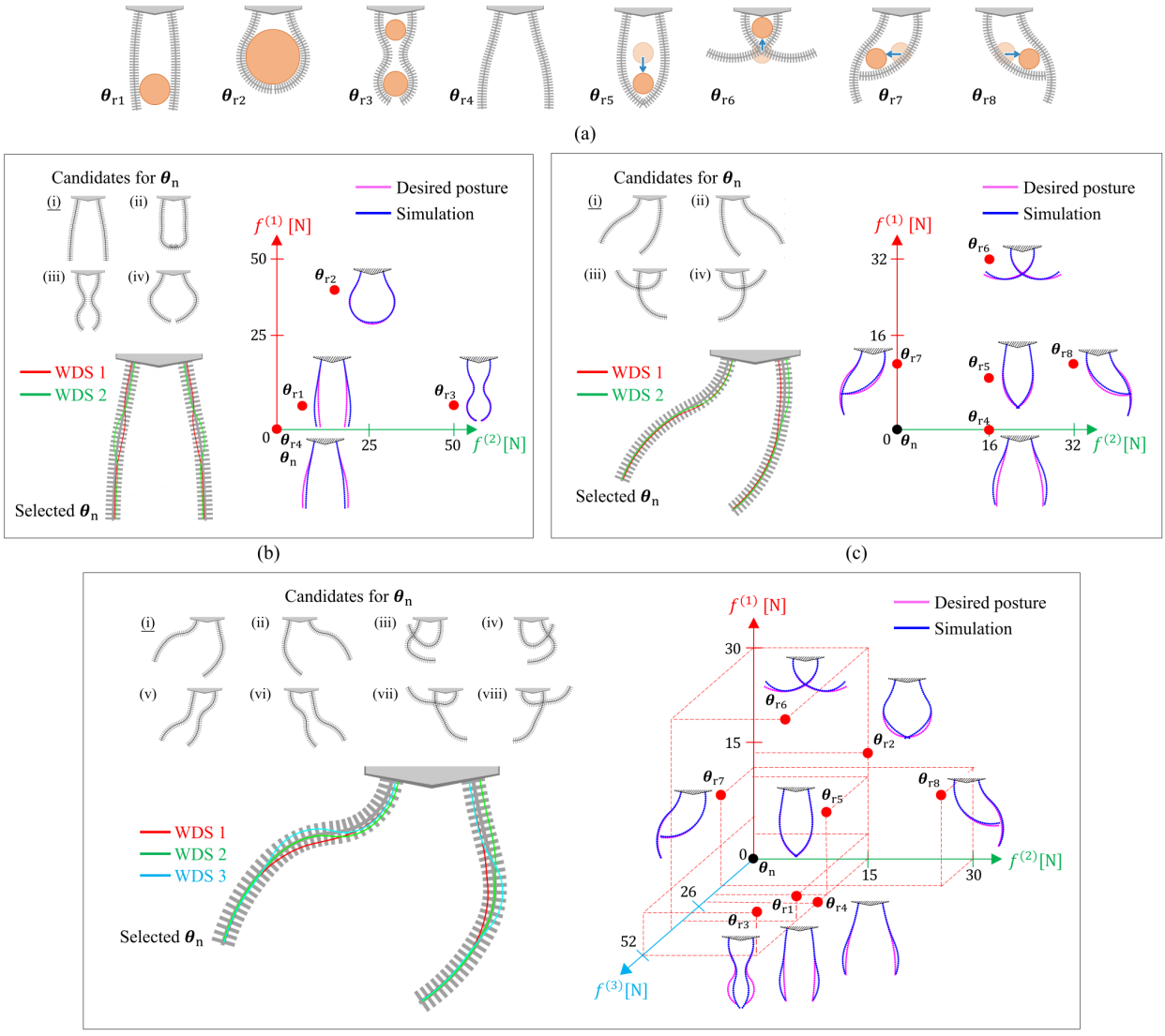

Fig. 5. Case studies. (a) Pool of desired postures ($\boldsymbol{\theta}_{\mathrm{r}1}$–$\boldsymbol{\theta}_{\mathrm{r}8}$). (b) Design for multi-mode grasping task with $\boldsymbol{\theta}_{\mathrm{r}1}$–$\boldsymbol{\theta}_{\mathrm{r}4}$ (Case 1). (c) Design for in-hand manipulation task with $\boldsymbol{\theta}_{\mathrm{r}4}$–$\boldsymbol{\theta}_{\mathrm{r}8}$ (Case 2). (d) Design for the above two tasks with $\boldsymbol{\theta}_{\mathrm{r}1}$–$\boldsymbol{\theta}_{\mathrm{r}8}$ (Case 3). In (b), (c), and (d), candidates of natural posture $\boldsymbol{\theta}_{\mathrm{n}}$ are shown in the upper left. The selected natural posture and WDSs are shown in the lower left. The relationship between the wire tensions, desired postures, and reproduced postures in simulation are shown in the right.

1. As shown in TABLE I, the minimum number of inputs overcoming $R_{\mathrm{th}} = 0.95$ was $V = 2$ with $R_{\mathrm{cum},2} = 0.98$; thus, the number of WDSs was determined as $M = 2$. Fig. 5(c) shows the design results. $2^V = 4$ candidates for $\boldsymbol{\theta}_{\mathrm{n}}$ were obtained as shown in the top left of Fig. 5(c). Based on TABLE II, candidate (i) for Case 2 was selected, as shown in the bottom left of Fig. 5(c). The red and green lines in the bottom left of Fig. 5(c) indicate the passage points for WDS 1 and WDS 2, respectively. The relationship between the tensions $f^{(1)}$ and $f^{(2)}$, the desired postures $\boldsymbol{\theta}_{\mathrm{r}4}$–$\boldsymbol{\theta}_{\mathrm{r}8}$, and the reproduced postures in simulation are shown in the right of Fig. 5(c). The coefficient matrix was $\boldsymbol{A} = \mathrm{diag}[1.4, 1.7]$.

3) Case 3: Design for Two Tasks: Assuming a hand that performs both tasks in Cases 1 and 2, we designed a hand for eight desired postures $\boldsymbol{\theta}_{\mathrm{r}1}$–$\boldsymbol{\theta}_{\mathrm{r}8}$, as shown in Fig. 5(a). As shown in TABLE I, the minimum number of inputs overcoming $R_{\mathrm{th}} = 0.95$ was $V = 3$ with $R_{\mathrm{cum},3} = 0.96$; thus, the number of WDSs was determined as $M = 3$. Fig. 5(d) shows the design results. $2^V = 8$ candidates for $\boldsymbol{\theta}_{\mathrm{n}}$ were obtained as shown in the top left of Fig. 5(d). Based on TABLE II, candidate (i) for Case 3 was selected, as shown in the bottom left of Fig. 5(d). The red, green, and cyan lines in the bottom left of Fig. 5(d) indicate the passage points for WDS 1, WDS 2, and WDS 3, respectively. The relationship between the tensions $f^{(1)}$–$f^{(3)}$, the desired postures $\boldsymbol{\theta}_{\mathrm{r}1}$–$\boldsymbol{\theta}_{\mathrm{r}8}$, and the reproduced postures in the simulation are shown in the right of Fig. 5(d). The coefficient matrix was $\boldsymbol{A} = \mathrm{diag}[1.3, 1.6, 5.4]$.

The reproduced postures of the hand designed using the proposed method included errors due to the linearization with respect to the posture $\boldsymbol{\theta}$ and the dimensionality reduction of input. Nevertheless, the reproduced postures in Cases 1–3 qualitatively corresponded to the desired postures, as shown in Figs. 5(b)–(d). In Case 1, however, despite the cumulative

TABLE II

MAXIMUM AND AVERAGE ANGLES OF $|\theta_{\mathrm{n},i}|$ $(i = 1, \ldots, 70)$.

		(i)	(ii)	(iii)	(iv)	(v)	(vi)	(vii)	(viii)
Case 1	$\lvert\theta_{\mathrm{n},i}\rvert_{\max}$ °	1.0	9.5	8.7	7.8				
	$\lvert\theta_{\mathrm{n},i}\rvert_{\mathrm{avg}}$ °	0.4	4.9	6.2	4.3				
Case 2	$\lvert\theta_{\mathrm{n},i}\rvert_{\max}$ °	4.4	4.4	7.2	7.2				
	$\lvert\theta_{\mathrm{n},i}\rvert_{\mathrm{avg}}$ °	2.2	2.2	3.8	3.8				
Case 3	$\lvert\theta_{\mathrm{n},i}\rvert_{\max}$ °	6.6	6.6	12	12	6.8	6.8	9.4	9.4
	$\lvert\theta_{\mathrm{n},i}\rvert_{\mathrm{avg}}$ °	3.1	3.1	5.0	5.0	4.1	4.1	4.3	4.3

TABLE III

MAEs IN THE REPRODUCED POSTURES.

	MAE	$\boldsymbol{\theta}_{\mathrm{r}1}$	$\boldsymbol{\theta}_{\mathrm{r}2}$	$\boldsymbol{\theta}_{\mathrm{r}3}$	$\boldsymbol{\theta}_{\mathrm{r}4}$	$\boldsymbol{\theta}_{\mathrm{r}5}$	$\boldsymbol{\theta}_{\mathrm{r}6}$	$\boldsymbol{\theta}_{\mathrm{r}7}$	$\boldsymbol{\theta}_{\mathrm{r}8}$
Case 1	E_θ °	0.6	0.5	1.3	0.4				
	E_{p} mm	7.3	1.6	1.2	5.9				
Case 2	E_θ °				1.0	0.5	0.7	0.6	0.6
	E_{p} mm				8.2	2.3	3.2	5.0	5.1
	$E_{\mathrm{p,expD}}$ mm				15	3.0	12	4.1	6.4
	$E_{\mathrm{p,expS}}$ mm				8.5	4.2	11	6.4	8.3
Case 3	E_θ °	1.6	1.5	2.7	1.1	0.4	1.0	0.3	0.5
	E_{p} mm	5.0	4.2	7.0	4.2	0.8	3.2	1.3	2.6

contribution ratio being $R_{\mathrm{cum},2} = 0.98$, the errors for $\boldsymbol{\theta}_{\mathrm{r}1}$ and $\boldsymbol{\theta}_{\mathrm{r}4}$ were not small, as shown in Fig. 5(b). TABLE III shows the mean absolute errors (MAEs) between the reproduced and desired postures, where E_θ is the MAE for joint angular displacement and E_{p} is that for joint position. In Cases 1–3, E_θ was within 3.0 °, and E_{p} was within 10 mm which was half the length of branch $d = 20$ mm.

In Case 1, the natural posture $\boldsymbol{\theta}_{\mathrm{n}}$ and passage points for WDS 1 and WDS 2 were symmetrical, as all desired postures were symmetrical. In contrast, in Case 2, the natural posture $\boldsymbol{\theta}_{\mathrm{n}}$ and passage points for WDS 1 and WDS 2 were asymmetrical because the asymmetrical desired postures were included. The proposed method can analytically determine such complex hand mechanisms without using iterative calculations or machine learning. Thus, it simplifies and expediates the design process. In the above case studies, the hands were designed to reproduce various desired postures despite the number of WDSs at most two or three. While the hands in Cases 1 and 2 were designed with $M = 2$, the hand in Case 3, which combined both tasks, was designed not with $M = 2 + 2 = 4$, but with $M = 3$. This result suggests that the proposed method can design a hand reproducing desired postures efficiently with fewer actuators.

V. EXPERIMENTS

The feasibility of the proposed method was verified via experiments, which are shown in the supplementary video.

A. Developed Hand

Fig. 6(a) shows an overview of the developed hand designed for Case 2, described in Section IV. The wire passages and natural posture were the same as those shown in Fig. 5(c). The finger trunks and branches, wire passages, and natural posture were produced by using 3D CAD, and fabricated using 3D printing. The finger and wire were made of polylactic acid (Pxmalion PLA) and nylon (fishing line), respectively. Fig. 6(b) shows the detailed top and side views

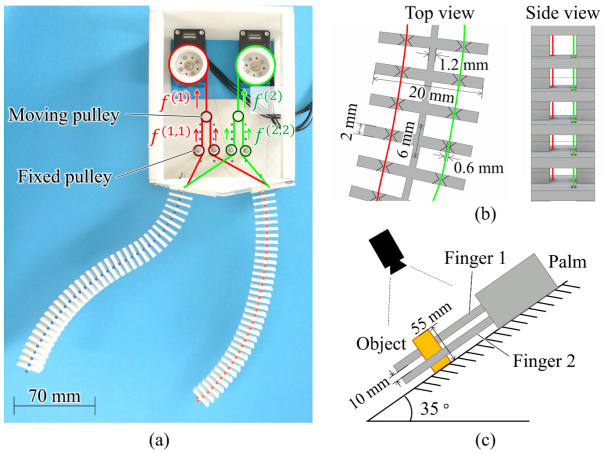

Fig. 6. Developed hand. (a) Overview. (b) Top and side views. (c) Experimental environment.

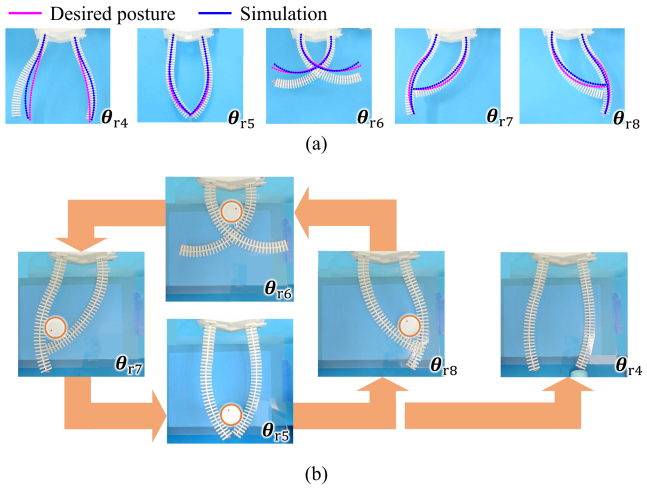

Fig. 7. Experimental results. (a) Reproduction of the desired postures. (b) Performance of the in-hand manipulation task.

of the finger. The width of the wire passages was 0.6 mm, and the wire diameter was 0.33 mm. Two wires did not interfere with each other as they were located at the front and back sides of the finger. Two motors (Dynamixel XM430-W350-R) to reel the wire were assembled on the palm, as shown in Fig. 6(a). Additionally, a tension equalizing mechanism comprising a moving pulley and fixed pulleys was equipped. This mechanism ensured that the two wires passing through the hand were parallel to the wire reeled by the motor in the same WDS. When a tension $f^{(m)}$ was applied on the wire of motor, an equal tension $f^{(m)}/2$ was distributed to the wire of each finger. The tension was controlled by monitoring the current applied to the motor. The right finger was displaced 10 mm in depth from the left finger; consequently, the fingers did not come into contact. Colored markers were attached to joint positions so that the hand posture can be measured via image processing.

B. Reproduction of Desired Postures

Fig. 7(a) shows the hand postures on a horizontal plane when giving the tension $\boldsymbol{f} = [f^{(1)}, f^{(2)}]^{\mathrm{T}}$ for reproducing the desired postures $\boldsymbol{\theta}_{rh}$ shown in the right of Fig. 5(c). The magenta and blue lines in Fig. 7(a) are the desired and simu-

lation postures, respectively. While the experimental postures reproduced by the developed hand qualitatively corresponded to the desired postures, its error have the same tendency with those of simulation which has the same design parameters. $E_{\mathrm{p,expD}}$ and $E_{\mathrm{p,expS}}$ in TABLE III are the MAEs of joint position for experimental postures with respect to desired and simulation postures, respectively. Possible reasons for the errors are the following: the bending elasticity might include non-linear components, and the friction between the wire and passage, neglected in the analysis, might cause a variation in the tension. Compensation for them should be considered.

C. Performing the In-hand Manipulation Task

Fig. 7(b) shows the experiment of in-hand manipulation using $\boldsymbol{\theta}_{\mathrm{r5}}$–$\boldsymbol{\theta}_{\mathrm{r8}}$ in Fig. 5(a). A cylindrical melamine sponge was used as the object, where the diameter was $33\ \mathrm{mm}$, the depth was $55\ \mathrm{mm}$, the mass was $3.0\ \mathrm{g}$, and the static friction coefficient between the hand and object was 0.3. This experiment was conducted in the environment with the inclination as shown in Fig. 6(c). In this environment, the object was affected by gravity while it was restrained to a two-dimensional plane. First, the hand posture was set to $\boldsymbol{\theta}_{\mathrm{r5}}$ to grasp the object. Then, it was changed in the order $\boldsymbol{\theta}_{\mathrm{r5}} \to \boldsymbol{\theta}_{\mathrm{r8}} \to \boldsymbol{\theta}_{\mathrm{r6}} \to \boldsymbol{\theta}_{\mathrm{r7}} \to \boldsymbol{\theta}_{\mathrm{r5}}$ to move the object around in the hand. Finally, it was set to $\boldsymbol{\theta}_{\mathrm{r4}}$ to release the object.

This experiment was simple and qualitative. However, the inverse problem of designing and developing a hand, which performs a task by reproducing desired postures, was solved, and the task was successfully executed. Thus, the task-oriented approach in Fig. 1(b) was conducted, which verified the feasibility of the proposed method.

VI. Conclusions

This paper discussed a task-oriented design for wire-driven flexible hands. The main results are summarized as follows:

- Supposing the fabrication using 3D printing, an analytical model of a monolithic hand with wire drive systems was introduced. Then, the wiring-synergy equation was derived, which relates the mechanism parameters, wire tension, and generated posture.
- The posture-synergy equation for desired postures given to perform a task was derived via PCA. Based on the isomorphism in the two synergy equations, a design method for a hand was constructed. Under the posture reproducibility with respect to the number of WDSs, this method can analytically determine the mechanism parameters and wire tension for desired postures.
- The proposed method was validated through the case studies for multi-mode grasping, in-hand manipulation, and both of these tasks. In addition, the hand for the in-hand manipulation task was developed, and the feasibility of the proposed method was experimentally validated.

Although the proposed method develops a hand for a specific task without high versatility, it potentially contributes to expediting the design procedure, increasing the accuracy of performing task, and reducing the number of actuators. The proposed method determines the mechanism parameters and assesses the posture reproductivity, based on a mathematical analysis for desired postures. As discussed in Sections III and IV, inappropriate mechanism parameters and posture errors that cannot be understood using the cumulative contribution ratio may result in the real system. To address such cases systematically, we should discuss the existence and validity of the solutions in detail from a physical perspective. Future works include a design problem considering gravitational force, contact force, and frictional force.

References

[1] A. Bicchi, "Hands for Dexterous Manipulation and Robust Grasping: A Difficult Road Toward Simplicity," IEEE Trans. on Robotics and Automation, vol. 16, no. 6, pp. 652–662, 2000.

[2] D. Prattichizzo and J. Trinkle, "Grasping: in Handbook on Robotics," B. Siciliano and O. Kathib, Eds. Springer, pp. 671–700, 2008.

[3] J. Shintake, V. Cacucciolo, D. Floreano, and, H. Shea, "Soft Robotic Grippers," Advanced Materials, vol. 30, no. 29, 1707035, 2018.

[4] D. J. Sut and P. Sethuramalingam, "Soft Manipulator for Soft Robotic Applications: a Review," Journal of Intelligent and Robotic Systems, vol. 108, article number 10, 2023.

[5] R. Deimel and O. Brock, "A Compliant Hand Based on a Novel Pneumatic Actuator," Proc. of the IEEE Int. Conf. on Robotics and Automation, pp. 2047–2053, 2013.

[6] N. Feng, Q. Shi, H. Wang, J. Gong, C. Liu, and Z. Lu, "A Soft Robotic Hand: Design, Analysis, sEMG Control, and Experiment," Int. J. of Advanced Manufacturing Technology, vol. 97, pp. 319–333, 2018.

[7] Z. Wang, Y. Torigoe, and S. Hirai, "A Prestressed Soft Gripper: Design, Modeling, Fabrication, and Tests for Food Handling," IEEE Robotics and Automation Letters, vol. 2, no. 4, pp. 1909–1916, 2017.

[8] M. Manti, T. Hassan, G. Passetti, N. D'Elia, C. Laschi, and M. Cianchetti, "A Bioinspired Soft Robotic Gripper for Adaptable and Effective Grasping," Soft Robotics, vol. 2, no. 3, pp. 107–116, 2015.

[9] A. Qiu, C. Young, A. L. Gunderman, M. Azizkhani, Y. Chen, and A-P. Hu, "Tendon-Driven Soft Robotic Gripper with Integrated Ripeness Sensing for Blackberry Harvesting," Proc. of the IEEE Int. Conf. on Robotics and Automation, pp. 11831–11837, 2023.

[10] K. Hsiao and H. Mochiyama, "A Wire-driven Continuum Manipulator Model without assuming Shape Curvature Constancy," Proc. IEEE/RSJ Int. Conf. Intelligent Robots Systems, pp. 436–443, 2017.

[11] H. Yuan, Z. Li, and W. Xu, "Kinetostatics for Variable Cross-section Continuum Manipulators," Proc. of the IEEE Int. Conf. on Robotics and Automation, pp. 11878–11883, 2021.

[12] G. Salvietti, Z. Iqbal, M. Malvezzi, T. Eslami, and D. Prattichizzo, "Soft Hands with Embodied Constraints: The Soft ScoopGripper," Proc. of the IEEE Int. Conf. on Robotics and Automation, pp. 2758–2764, 2019.

[13] T. Onodera, N. Iwamoto, and T. Umedachi, "In-Hand Manipulation Exploiting Bending and Compression Deformations of Caterpillar-Locomotion-Inspired Fingers," Proc. IEEE/RSJ Int. Conf. Intelligent Robots Systems, pp. 1188–1195, 2022.

[14] Y. S. Krieger, S. Schiele, S. Detzel, C. Dietz, and T. C. Lueth, "Shape Memory Structures - Automated Design of Monolithic Soft Robot Structures with Pre-defined End Poses," Proc. of the IEEE Int. Conf. on Robotics and Automation, pp. 9357–9362, 2019.

[15] S. Schiele, H. Phalen, J. Kulozik,Y. S. Krieger, and T. C. Lueth, "Automated Design of Underactuated Monolithic Soft Robotics Structures with Multiple Predefined End Poses," Proc. of the IEEE Int. Conf. on Robotics and Automation, pp. 6868–6874, 2021.

[16] M. Dragusanu, G. M. Achilli, M. C. Valigi, D. Prattichizzo, M. Malvezzi, and G. Salvietti, "The WaveJoints: A Novel Methodology to Design Soft-Rigid Grippers Made by Monolithic 3D Printed Fingers with Adjustable Joint Stiffness," IEEE Int. Conf. on Robotics and Automation, pp. 6173–6179, 2022.

[17] Y. Watanabe and M. Higashimori, "Synergy-Based Analytical Design of Wire-Driven Continuum Manipulators," IEEE Robotics and Automation Letters, vol. 7, no. 4, pp. 9310–9317, 2022.

[18] G. Grioli, M. Catalano, E. Silvestro, S. Tono, and A. Bicchi, "Adaptive Synergies: An Approach to the Design of Under-actuated Robotic Hands," Proc. IEEE/RSJ Int. Conf. Intell. Robots Syst., pp. 1251–1256, 2012.